ELSEVIER

www.elsevier.nl/locate/jorganchem

Journal of Organometallic Chemistry 622 (2001) 97–111

Journal of Organometallic Chemistry

Cationic chelate phosphane substituted carbyne tungsten complexes

Ewald Bannwart, Heiko Jacobsen, Rainer Hübener, Helmut W. Schmalle, Heinz Berke *

Anorganisch-Chemisches Institut der Universität Zürich, Winterthurerstrasse 190, CH–8057 Zürich, Switzerland

Received 15 June 2000; received in revised form 21 September 2000; accepted 25 October 2000

Abstract

Reaction of $W(CMes)Cl(CO)_2(dppe)$ (**1**) and $W(CMes)Cl(CO)(dppep)$ (**8**) (Mes = 2,4,6-trimethylphenyl, dppe = $Ph_2PCH_2CH_2PPh_2$, dppep = $(Ph_2PCH_2CH_2)_2PPh$) with $AgSbF_6$ or AgOTf ($OTf = CF_3SO_3^-$) as halide abstraction reagents affords $[W(CMes)(CO)_n(Y)][X]$; (**2**): Y = dppe, $n = 2$; (**9**): Y = dppep, $n = 1$; (**a**) $X = SbF_6^-$; (**b**): X = OTf. In solution, the metal moieties of compounds **2a**, **9a** and **9b** exist as naked cations, which possess a square pyramidal coordination. The carbyne ligand occupies the apical position, and a free coordination site is located *trans* to the CMes group. The reaction of **2a** with a variety of donor ligands leads to $[W(CMes)(CO)_2(dppe)L][SbF_6]$ compounds, in which the ligand L binds *trans* to the carbyne unit (L = THF (**4a**), CH_3CN (**4b**), PMe_3 (**5a**), PEt_3 (**5b**)). In the carbonyl adducts $[W(CMes)(CO)_n(Y)][SbF_6]$; Y = dppe, $n = 3$, (**3**); Y = dppep, $n = 2$, (**10**); the chelating ligands rearrange so that a phosphorus donor atom coordinates *trans* to the carbyne ligand. The reaction of **2a** with $P(OMe)_3$ and $P(OEt)_3$ results in the phosphonate complexes $[W(CMes)(CO)_2(OPH(OR)_2)(dppe)][SbF_6]$; R = Me (**6a**), Et (**6b**), which are formed in an Arbuzov dealkylation reaction. When **1** is reacted with a deficient amount of silver salt, the bimetallic complex $[\{W(CMes)(CO)_2(dppe)\}_2Cl][SbF_6]$ (**7**) is obtained. The unusual molecular geometries of **6a** and **7** were confirmed by a crystal structure determination. A theoretical analysis reveals the importance of electrostatic interaction for ligand bonding with the cationic metal fragments.

Keywords: Triple bonded ligand system; Metal center; Carbyne tungsten complexes

1. Introduction

In transition metal coordination chemistry, the carbyne moiety CR acts as a triple bonded ligand system, and establishes very close contacts to the metal center [1]. As a consequence, it exhibits a strong influence on ligands $L^{t\text{-}CR}$ disposed in *trans* position [2]. The *trans*-effect substantially labilizes the $M–L^{t\text{-}CR}$ bond, or even prevents coordination of a *trans*-ligand [1], resulting in electronically unsaturated $16e^-$ carbyne complexes. In order to exploit the characteristic features of the CR group, we approached the synthesis of bi- and tridentate phosphane substituted tungsten carbyne complexes [3,4]. The electron donating phosphorus ligands were supposed to account for some compensation of the electronic deficiency of $16e^-$ species, and their chelating properties were sought to stabilize the coordination sphere around the transition metal center.

The underlying motivation for the design of such complexes originated from the idea that catalytic transformations mediated by transition metal complexes generally require labile coordination sites. The carbyne ligand might provide the lability needed, and render the tungsten complex catalitically active.

In this work, we describe the synthesis of the cationic tungsten carbyne complexes $[W(CMes)(CO)_2(dppe)]^+$ and $[W(CMes)(CO)(dppep)]^+$ as potential precursors for catalytic conversions (Mes = 2,4,6-trimethylphenyl, dppe = $Ph_2PCH_2CH_2PPh_2$, dppep = $(Ph_2PCH_2CH_2)_2PPh$). We further initiated an investigation of their reactivity by exploring the coordination behavior of these cations towards prototypical donor ligands. The reactivity studies are supported by theoretical calculations based on density functional theory (DFT) [5].

* Corresponding author. Tel.: +41-1-635-4680; fax: +41-1-635-6802.

E-mail address: hberke@aci.unizh.ch (H. Berke).

0022-328X/01/$ - see front matter
PII: S0022-328X(00)00864-0

2. Results and discussion

2.1. Synthesis and reactivity of $[W(CMes)(CO)_2(dppe)]^+$ complexes

A synthetic route to dppe substituted tungsten carbyne cations has been described before in the literature. The groups headed by Templeton [6] and Gimeno [7] introduced the carbyne unit by protonation of the corresponding vinylidene compounds. These systems, however, seemed not to be suitable precursors for coordinatively unsaturated species, since one might suspect that the inevitable presence of α-hydrogens at the carbyne residue could eventually cause complications in the preparation of $16e^-$ complexes. We therefore intended to develop aryl carbyne species, which were obtained in the reaction of carbyne chloride complexes with silver salts, acting as halide abstraction reagents.

2.1.1. Preparation of $[W(CMes)(CO)_2(dppe)]^+$

Starting point for the synthesis of tungsten cations containing the dppe ligand was the complex $W(CMes)(CO)_2Cl(dppe)$ (**1**), which we have described earlier in the context of the synthesis of carbyne hydride species [3]. The reaction of **1** with a slight excess of $AgSbF_6$ in CH_2Cl_2 affords the naked cation $[W(CMes)(CO)_2(dppe)]^+$ (**2a**) as SbF_6^- salt (Scheme 1).

The conversion proceeds smoothly at room temperature, and is complete within minutes. When keeping **2a** in solution, decomposition is observed already after a short period of time. One of the decomposition products could be identified as the triply carbonyl substituted cation **3** (vide infra). In the solid state, however, **2a** appears to be more stable. It can be stored without decomposition for an indefinite period of time at −20°C.

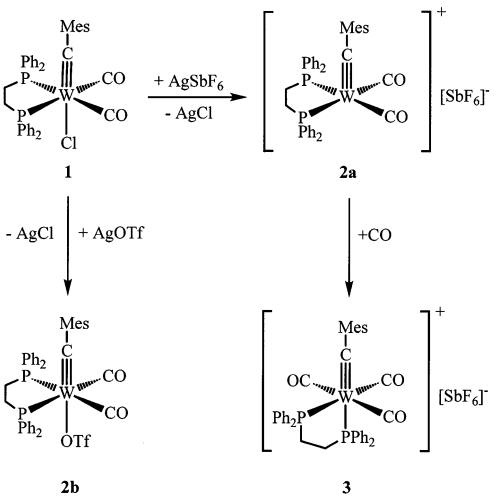

Scheme 1.

The reaction of **1** with $AgSbF_6$ can be monitored in the IR spectrum through the appearance of two new, intense ν(CO) bands at 2006 and 1940 cm^{-1}. These signals are shifted to higher wavenumbers as compared to those for **1**, which are found at 1997 and 1913 cm^{-1}, respectively. The high field shift observed in the carbonyl stretching frequencies is caused by electrostatic contributions to the [M]–CO bond [8,9], and provides a first indication to the cationic nature of the transition metal moiety. The intensity pattern of the ν(CO) bands suggests that the CO groups are coordinated in *cis* position to each other.

The only signal observed in the $^{31}P\{^1H\}$-NMR spectrum is a singlet resonance at 50.7 ppm with a $^1J_{PW}$ coupling constant of 237 Hz; a value characteristic of phosphorus donors in *trans* position to a carbonyl ligand [10,11]. This points to the fact that the P-atoms of the dppe group and the CO ligands are located in the same coordination plane. Further evidence for this finding is provided by the $^{13}C\{^1H\}$-NMR spectrum, in which the chemically equivalent C_{CO} atoms are identified as doublet of a doublet at 207.5 ppm. The two $^2J_{CP}$ values are 36.5 and 5.0 Hz, and are due to P nuclei in *trans* and in *cis*-position, respectively. The resonance for the C_{CMes} atom is found at 300 ppm, and is significantly shifted to lower field by 29 ppm, compared to the corresponding signal measured for **1**. These spectroscopic findings, together with a dominant M^+ peak at $e/z = 769$ in the mass spectrum, unequivocally confirm the square pyramidal coordination geometry of the $16e^-$ cation **2a**. The prominent axial position is occupied by the carbyne ligand.

A coordination of hexafluoroantimonate in **2a** can be definitely excluded. $^{31}P\{^1H\}$-NMR spectra recorded at various temperatures do not reveal any $^2J_{FP}$ coupling, as would be expected in the case of coordination of the counter ion [12]. Furthermore, only one band for the Sb–F stretches is observed at 665 cm^{-1} in the IR spectrum. A monodentate SbF_6^- group, however, is characterized by the presence of three ν(SbF) bands [13].

When silver trifluoromethanesulfonate AgOTf ($OTf = CF_3SO_3^-$) is used as halide abstraction reagent, compound **2b** is obtained as yellow powder in good yield (Scheme 1). The ν(CO) stretching frequencies appear at 1998 and 1932 cm^{-1}, and the value for the ^{13}C-resonance of the C_{CMes} atom is determined as 289.6 ppm. When these values are compared with the corresponding data for compounds **1** and **2a**, the metal center in **2b** seems to have less cationic character than in **2a**, but still carries a higher amount of positive charge than in **1**. These findings point to the presence of a weakly coordinated OTf group in **2b**; a fact that is supported by three additional observations. When NaOTf is added to a solution of **2b**, a new signal appears in the ^{19}F-NMR spectrum. This new resonance,

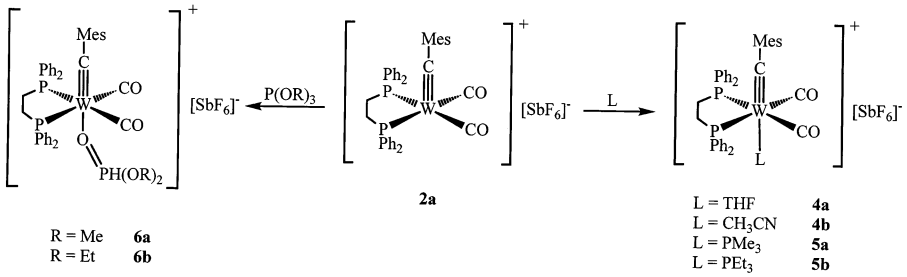

Scheme 2.

which is attributed to a free triflate anion, is shifted to higher field compared to the ^{19}F-resonance at -78 ppm for **2b**, which is due to coordinated OTf. Secondly, for the free triflate anion, the S–O stretching frequencies have been determined as $\nu_{as}(SO_3) = 1273$ and $\nu_s(SO_3) = 1032$ cm^{-1} [14], whereas for **2b**, values of 1204 and 1007 cm^{-1} have been measured. The shift to lower wavenumbers indicates a weakening of the S–O bond, caused by coordination of the OTf group to the metal center. Finally, a peak at $e/z = 920$ in the mass spectrum confirms the existence of a cation with the composition $C_{39}H_{35}F_3O_5P_2SW$. The patterns for the dppe and carbonyl ligands in the ^{31}P{^{1}H}- and ^{13}C{^{1}H}-NMR spectra are in qualitative agreement with those for **2a**. Compound **2b**, therefore, possesses a pseudo octahedral coordination geometry with the carbyne and the triflate groups in *trans*-, and the carbonyl ligands in *cis*-position.

2.1.2. Reaction of $[W(CMes)(CO)_2(dppe)]^+$ with carbon monoxide

The triply carbonyl-substituted cation **3**, which appears during the decomposition of **2a** in solution, can be obtained in almost quantitative yield, when the reaction of **1** with $AgSbF_6$ is carried out under an atmosphere of carbon monoxide (Scheme 1). The formation of the new compound is seen in the IR spectrum by the appearance of three new ν(CO) bands at 2074, 1993, and 1922 cm^{-1}. Alternatively, **2a** might be dissolved in a non-coordinating solvent, and stirred for a few minutes under 1 atm of CO. **3** is isolated as bright-yellow powder, and contrary to **2a**, it is stable also in solution at room temperature.

The ^{13}C-resonance of the C_{CMes} atom appears at 308.6 ppm as doublet of a doublet with $^2J_{CP}$ values of 20.4 and 7.7 Hz, where the large coupling constant is due to interaction with a P-nucleus in *trans* position. In the ^{31}P{^{1}H}-NMR spectrum, two signals at 37.9 and 23.9 ppm are observed, which both exhibit tungsten satellites with $^1J_{PW}$ couplings of 237 and 91 Hz, respectively. The remarkably small $^1J_{PW}$ value for the signal at higher field can be attributed to a phosphorus donor coordinated in *trans* position to a carbyne group [6b,7] The $^2J_{PP}$ coupling of the chemically non equivalent phosphorus atoms is too small to be resolved in the ^{31}P{^{1}H}-NMR spectrum; an observation which was made before by Templeton [6] and Gimeno [7] for analogous compounds.

From the spectroscopic data discussed above together with the ^{13}C-resonances of the carbonyl ligands, one can deduce the coordination geometry for the cation **3**. The complex possesses a pseudo octahedral coordination sphere, in which one of the P atoms of the dppe ligand is located *trans* to the carbyne group. The remaining P atom and three carbonyl groups define a meridional plane in this complex.

The fact that a carbon monoxide molecule does not occupy the free coordination site *trans* to the carbyne moiety in **2a** underlines the strong *trans* influence of the CMes group. Due to the strong [W]≡CMes triple bond, the tungsten center cannot provide enough electron density for π-backdonation to support a stable [W]–CO bond in *trans* position.

The incoming CO ligand does not show a preference for one specific coordination site. When the reaction of **1** with $AgSbF_6$ is performed under an atmosphere of ^{13}C-labeled carbon monoxide, both carbonyl resonances in the ^{13}C-NMR spectrum reveal the presence of ^{13}CO ligands. The intensity ratio of the two signals is approximately 1:1. When the ^{13}C-enriched complex **3** is treated with tetramethylammonium chloride, an equal mixture of labeled and unlabeled **1** is obtained. This reaction sequence offers the possibility of synthesizing isotopically labeled starting material.

2.1.3. Solvent complexes of $[W(CMes)(CO)_2(dppe)]^+$

When compounds **2a** or **3** are dissolved in deuterated THF, the NMR spectra reveal the existence of a new compound **4a** (Scheme 2), which is present in solution together with cations **2a** and **3**.

The yield of product formation has been determined as 20% by integration of the ^{31}P{^{1}H}-NMR signals. The small concentration of **4a** in the reaction mixture might be one of the reasons why the C_{CMes} resonance for the new compound could not be detected. Nevertheless, the new signals for the dppe and CO ligands at 47.1 and 218.5 ppm, as well as the presence of a coordinated THF molecule, indicated by low field shifts

of 1.2 and 2.7 ppm of the methylenic quintet resonances, provide evidence for a $[W(CMes)(CO)_2(dppe)(THF)]^+$ cation, in which the solvent molecule occupies the coordination site in *trans* position to the carbyne group.

It was not possible to isolate complex **4a**. Evaporation of excess solvent always led to loss of coordinated THF, and various attempts to crystallize or to precipitate **4a** were not successful.

Expectedly, a stable solvent complex can be obtained with the stronger donor acetonitrile. When the reaction of **1** and $AgSbF_6$ is carried out in a 3:1 mixture of dichloromethane and CH_3CN, the cationic complex $[trans\text{-}W(CMes)(CO)_2(dppe)(NCCH_3)]$ $[SbF_6]$ **4b** (Scheme 2) is isolated as yellow powder in almost quantitative yield. Even in solution, in the absence of stronger donor molecules, no dissociation of acetonitrile is observed. This reaction provides further opportunity to protect the cationic complex **2a** against decomposition.

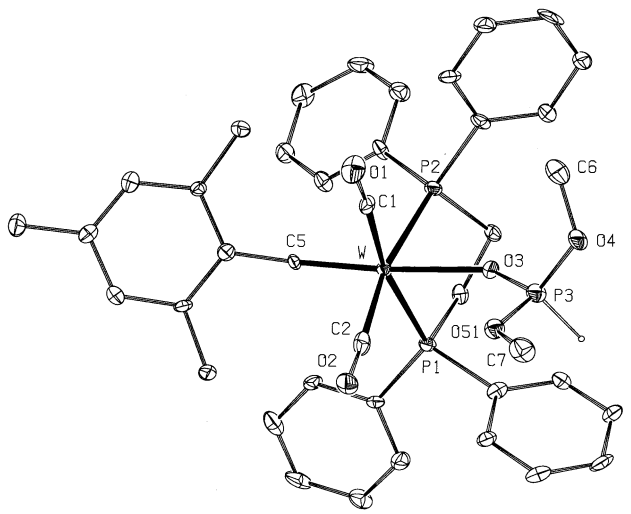

Fig. 1. The molecular structure of cation **6a** in the crystal. Disordered atoms and hydrogen atoms, except for H3 bound to P3, are omitted for clarity. Displacement ellipsoids are shown at the 30% level. H3 is dislayed as a sphere of arbitrary size. Selected bond distances (pm) and angles (°): W–C(5), 185.1(10); W–C(1), 202.3(12); W–C(2), 202.9(14); W–O(3), 225.0(8); W–P(2), 254.8(3); W–P(1), 256.4(3); P(3)–O(3), 146.5(8); P(3)–O(4), 155.5(8); P(3)–O(51), 158.0(10); P(3)–O(52), 170(8); P(3)–H(3), 144.9(3); O(1)–C(1), 113.9(14); O(2)–C(2), 112.7(15); O(4)–C(6), 146.3(16); O(51)–C(7), 142.3(16); O(52)–C(7), 141(9); C(5)–W–C(1), 84.3(4); C(5)–W–C(2), 86.9(5); C(1)–W–C(2), 90.9(5); C(5)–W–O(3), 172.4(4); C(1)–W–O(3), 88.2(4); C(2)–W–O(3), 92.7(4); C(5)–W–P(2), 103.0(3); C(1)–W–P(2), 95.8(3); C(2)–W–P(2), 168.5(4); O(3)–W–P(2), 78.3(2); C(5)–W–P(1), 105.5(3); C(1)–W–P(1), 169.6(3); C(2)–W–P(1), 93.2(4); O(3)–W–P(1), 82.1(2); P(2)–W–P(1), 78.69(9); O(3)–P(3)–O(4), 115.0(5); O(3)–P(3)–O(51), 108.5(5); O(4)–P(3)–O(51), 107.8(5); O(3)–P(3)–O(52), 129(3); O(4)–P(3)–O(52), 111(3); O(3)–P(3)–H, 108.5(4); O(4)–P(3)–H, 108.2(4); O(51)–P(3)–H(3), 108.8; O(52)–P(3)–H(3), 75(3); P(3)–O(3)–W, 142.7(5).

2.1.4. Reaction of $[W(CMes)(CO)_2(dppe)]^+$ with phosphorus donors

The reactivity of **2a** towards a variety of phosphanes was also investigated. In these experiments, a solution of **2a** in toluene was treated with one equivalent of the PR_3 donor at -20°C, and slowly warmed to room temperature.

The reactions with the trialkylphosphanes PMe_3 and PEt_3 proceed as expected. The new phosphorus donor occupies the coordination site *trans* to the CMes moiety (Scheme 2). The compounds **5a** and **5b** have been characterized by NMR and IR spectroscopy. Besides the now familiar pattern for a meridial coordination of the dppe and CO ligands, new triplets for the PR_3 donors appear in the $^{31}P\{^1H\}$-NMR spectrum at -58.9 and -26.2 ppm for **5a** and **5b**, respectively. The small $^1J_{PW}$ coupling constants of 83 and 84 Hz again corroborate the *trans* disposition of the CMes and PR_3 groups.

Through inspection of the NMR spectra of complexes **6a** and **6b**, which were obtained in the reaction of **2a** with $P(OMe)_3$ and $P(OEt)_3$, respectively, it became clear that in these cases, the P-donors display an unusual coordination chemistry (Scheme 2). A single crystal analysis of compound **6a** proved helpful in clearifying the structure of this compound. The geometry of the cation **6a** is depicted in Fig. 1.

The tungsten center in **6a** possesses a pseudo octahedral coordination, and the motif of meridional coordination of the dppe and CO ligands is well established. The [W] ≡ CMes bond length amounts to 185.5(10) pm, and lies within the expected range for tungsten carbyne complexes.[16] The structure reveals that the $P(OMe)_3$ molecule has been transformed oxidatively into $OPH(OMe)_2$. This ligand coordinates via an oxygen atom to the tungsten center. The P-atom possesses tetrahedral coordination geometry; the H-atom position at this group has been located by difference electron density calculations.

The spectral data are in accord with the results of the crystal structure analysis. In the $^{31}P\{^1H\}$-NMR spectrum, the signal for the dppe ligand now appears as doublet at 49.1 ppm, with a coupling constant $^3J_{PP}$ of 6 Hz, and tungsten satellites with $^1J_{PW} = 236$ Hz. A new triplet signal with half the integrated intensity of the doublet arises at 19.1 ppm, again with a $^3J_{PP}$ value of 6 Hz. The signal does not possess any tungsten satellites; an indication that the corresponding P-nucleus is not coordinated to the metal center. In the ^{31}P-NMR spectrum, this resonance splits into two signals with a $^1J_{PH}$ coupling of 752 Hz. This value is in the range of the $^1J_{PH}$ values reported for the free $OPH(OMe)_2$ molecule.[16] The P-bounded proton appears as doublet at 5.22 ppm, with the same $^1J_{HP}$ coupling constant measured in the ^{31}P-NMR experiment. These observations confirm the presence of the dimethyl phosphonate ligand.

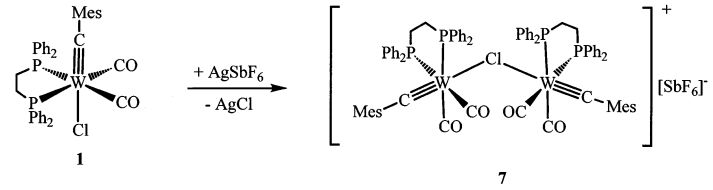

Scheme 3.

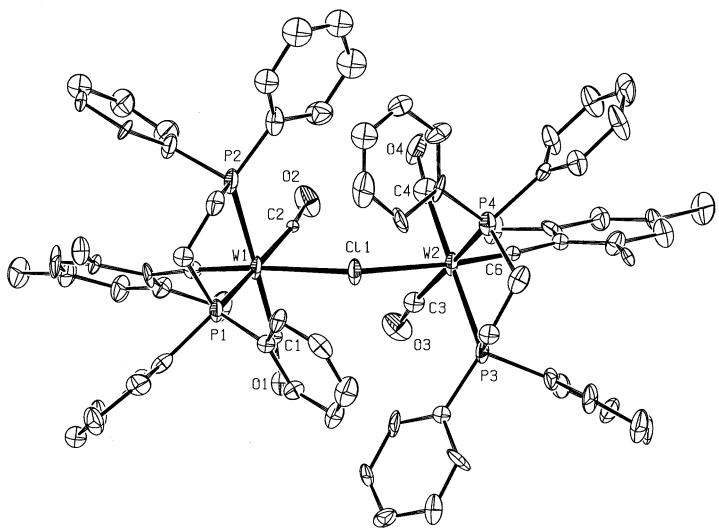

Fig. 2. The molecular structure of cation **7** in the crystal. Hydrogen atoms are omitted for clarity. Displacement ellipsoids are shown at the 30% level. Selected bond distances (pm) and angles (°): W(1)–C(1), 185(2); W(1)–C(2), 202(2); W(1)–C(5), 188(2); W(1)–P(1), 252.2(6); W(1)–P(2), 255.7(8); W(1)–Cl(1), 261.7(6); W(2)–C(3), 197(3); W(2)–C(4), 196(4); W(2)–C(6), 176.9(19); W(2)–P(3), 254.9(7); W(2)–P(4), 252.4(7); W(2)–Cl(1), 263.1(6); O(1)–C(1), 126(3); O(2)–C(2), 115(2); O(3)–C(3), 119(3); O(4)–C(4), 117(3); C(1)–W(1)–C(5), 88.0(9); C(1)–W(1)–C(2), 93.5(8); C(5)–W(1)–C(2), 86.6(8); C(1)–W(1)–P(1), 91.7(7); C(5)–W(1)–P(1), 98.8(7); C(2)–W(1)–P(1), 172.6(6); C(1)–W(1)–P(2), 170.0(6); C(5)–W(1)–P(2), 97.4(7); C(2)–W(1)–P(2), 95.2(6); P(1)–W(1)–P(2), 79.2(2); C(1)–W(1)–Cl(1), 84.4(6); C(5)–W(1)–Cl(1), 169.6(7); C(2)–W(1)–Cl(1), 86.7(5); P(1)–W(1)–Cl(1), 88.6(2); P(2)–W(1)–Cl(1), 91.2(2); C(6)–W(2)–C(4), 87.1(11); C(6)–W(2)–C(3), 91.6(9); C(4)–W(2)–C(3), 92.8(11); C(6)–W(2)–P(4), 97.2(7); C(4)–W(2)–P(4), 91.3(9); C(3)–W(2)–P(4), 170.4(7); C(6)–W(2)–P(3), 98.0(7); C(4)–W(2)–P(3), 170.0(9); C(3)–W(2)–P(3), 95.7(8); P(4)–W(2)–P(3), 79.5(2); C(6)–W(2)–Cl(1), 173.3(7); C(4)–W(2)–Cl(1), 86.9(9); C(3)–W(2)–Cl(1), 85.7(7); P(4)–W(2)–Cl(1), 85.9(2); P(3)–W(2)–Cl(1), 88.4(2); W(1)–Cl(1)–W(2), 126.4(3).

The spectroscopic data for compound **6b** comply with those of **6a**. This leads to the conclusion that a $OPH(OEt)_2$ ligand is present in the coordination sphere around the tungsten center.

The unexpected outcome of the reaction between **2a** and $P(OR)_3$ poses a question as to the mechanism of this transformation. Arbuzov-like [17] phosphite dealkylations of $P(OR)_3$ ligands have been reported before in the literature [18]. New, however, is the occurrence of phosphonic acid derivatives. NMR studies did not provide information about the fate of the cleaved methyl group, nor could the origin of the P-bounded proton be clarified as of yet. Traces of water as responsible impurities seem to be improbable since the reaction proceeds in a selective and reproducible manner, independent of the choice of solvent. Experiments in deuterated solvents also rule out the possibility that solvent molecules might act as proton donors.

2.2. The μ-Cl bridged dinuclear cation $[\{W(CMes)(CO)_2(dppe)\}_2Cl]^+$

The reaction of **2a** with halide abstraction reagents has also been performed with a deficient stoichiometry of the silver salt. During the reaction of **2a** with 0.5 equivalents of $AgSbF_6$, a complex product mixture develops after a few minutes. Besides the known compounds **1**, **2a**, and **3**, a new species **7** is detected in the $^{31}P\{^1H\}$-NMR spectrum (Scheme 3).

The yield of product formation, determined by integration of the ^{31}P-signals, amounts to ca. 40%. From a benzene solution of the product mixture, colorless crystals of **7** formed, which were suitable for an X-ray structure analysis.

The molecular geometry of cation **7** is displayed in Fig. 2. The dinuclear system comprises two $[W(CMes)(CO)_2(dppe)]^+$ units, bridged by a chloride anion.

The W–Cl distances amount to 261.7(6) and 263.1(6) ppm. These bonds are rather long when compared to the average [W]–(μCl) separation of 251 ppm [15]. The large tungsten–chloride distances indicate a weak W–Cl linkage, which is easily cleaved. It is not possible to detect **7** in solution without the presence of **1** and **2a**. The two tungsten moieties are not equivalent in the crystal; a fact that is suggested by the slight difference in the W–Cl lengths, and which is clearly seen when the tungsten–carbyne triple bonds are compared. The two [W] ≡ CR bonds of 188(2) and 176.9(19) pm differ by more than 10 pm. Also, the four [W]–CO) distances vary from 202(2) to 185(5) pm. The latter value is extremely short for a tungsten carbonyl bond, in comparison with average values of 202 and 200 pm for prototypical tungsten carbyne chlorides (vide infra). We will at a later point return to the molecular structure of **7**. One should however keep in mind that the poor quality of the crystals led to high *R*-values during the course of the structure determination, and that therefore the geometric parameters should be looked at with caution.

An asymmetric coordination around the bridging Cl^- is clearly supported by the $^{31}P\{^1H\}$-NMR spectrum. At low temperatures, two singlets are detected with $^1J_{PW}$ couplings around 230 Hz. The resonance at 40.7 ppm can be assigned to a complex with a short W–Cl bond, and is comparable to the value of 40.3 ppm for **1a**. The other signal appears at 44.7 ppm. The observed low field shift indicates a more cationic metal center, and a longer W–Cl separation. At temperatures around 0°C, coalescence sets in, and at room temperature, the two different sets of dppe ligands are equivalent on the NMR time scale. The fluctional behavior of the complex leads to one single ^{31}P-resonance at 42.5 ppm.

The preparation of **7** under an atmosphere of ^{13}CO provides further evidence for facile W-Cl bond breakage. All detected products **1**, **2a** **3**, and **7** contain labeled carbonyl ligands. The presence of ^{13}C-**1** might be explained by the reaction of ^{13}C-**2** with excess **1** to form the labeled compound ^{13}C-**7**. Dissociation of the dinuclear complex might then lead to ^{13}C-enriched starting material.

2.3. Synthesis and reactivity of $[W(CMes)(CO)(dppep)]^+$ complexes

2.3.1. Preparation of $[W(CMes)(CO)(dppep)]^+$

A second carbyne tungsten chloride with chelating phosphorus donors prepared earlier [3] is *trans*-$W(CMes)(CO)_2Cl(dppep)$ **8**. When this complex is reacted with either $AgSbF_6$ or AgOTf, a precipitate of AgCl is observed after a few minutes. In the IR spectrum, a new ν(CO) band appears, which in both cases is shifted by 90 cm^{-1} to higher wavenumbers. The spectroscopic data reveal the presence of the naked cation $[W(CMes)(CO)(dppep)]^+$, which can be isolated either as the hexafluoroantimonate salt **9a**, or as the triflate salt **9b** (Scheme 4).

In contrast to compound **2b**, the OTf anion does not coordinate to the tungsten center in cation **9b**. Besides the identical band for the ν(CO) stretch in the IR spectra of **9a** and **9b**, further evidence is furnished by the ν(SO) stretches at 1262 and 1032 cm^{-1}, which correspond to the literature values for the uncoordinated OTf ion [13] (vide supra). Furthermore, resonance of -78.7 ppm appears in ^{19}F-NMR spectrum, indicating the presence of free triflate. No new signals can be seen when sodium triflate is added to the NMR solution of **9b**. The five phenyl groups of the dppep introduce steric encumbrance, so that the free coordination site in the cation **9a** or **9b** is protected from coordination of sterically more demanding ligands.

Neither complex **9a** nor **9b** could be isolated in the purity required to obtain satisfactory elemental analysis. The complexes decompose, and in the reaction mixture, a doubly carbonyl substituted cation can be identified as a new compound.

2.3.2. Reactions of $[W(CMes)(CO)(dppep)]^+$

We conclude our experimental section with a concise report on exemplary reactivity studies that have been undertaken with compound **9a**. When the reaction between **8** and $AgSbF_6$ is carried out in the presence of carbon monoxide, complex **10** containing two carbonyl ligands is obtained (Scheme 4). The presence of two intense ν(CO) stretches reveal the *cis*-coordination of the CO ligands. In the $^{31}P\{^1H\}$-NMR spectrum, three signals for the chemically non-equivalent P-nuclei are

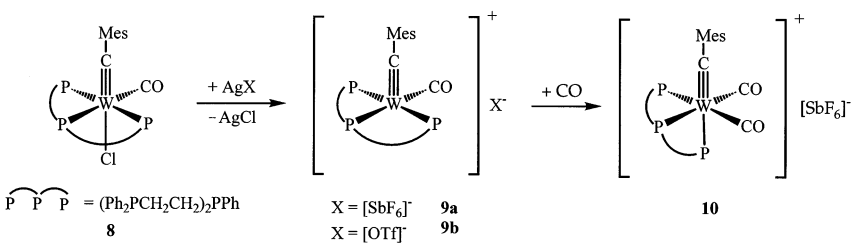

Scheme 4.

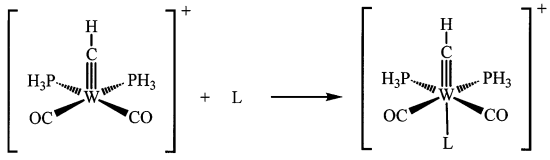

L = PH_3	**IIa**$^+$
L = PMe_3	**IIb**$^+$
L = $P(OH)_3$	**IIc**$^+$
L = $P(OMe)_3$	**IId**$^+$
L = CO	**IIe**$^+$
L = NCMe	**IIf**$^+$
L = THF	**IIg**$^+$
L= CH_2Cl_2	**IIh**$^+$
L=$OPH(OH)_2$	**IIi**$^+$

Scheme 5.

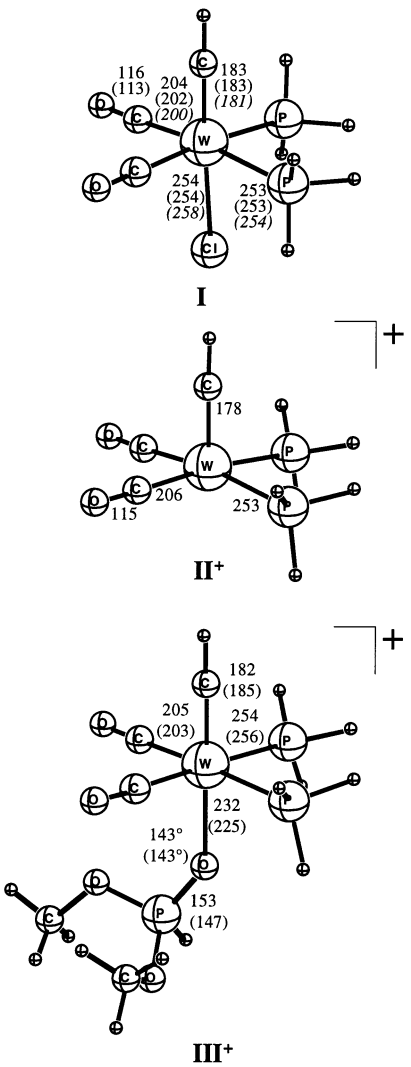

Fig. 3. Comparison of optimized model geometries **I**, **II**$^+$ and **III**$^+$, with experimental data of related compounds (in parentheses; averaged values). For **I**, values are taken from Refs. [7,19]. Distances are given in pm, angles in degrees.

seen, which are split into doublets of a doublet with $^2J_{PP}$ values smaller than 20 Hz, as can be expected for P-donor ligands in *cis* position [11]. One of the $^1J_{PW}$ coupling constants with a small value of 75 Hz is indicative of a P-nucleus in *trans* position to the carbyne group. The spectroscopic data suggest that the dppep ligand changes is coordination mode from a meridional to facial arrangement. The driving force is once again the pronounced *trans* influence of the carbyne moiety, which prevents a coordination of a strong π-acceptor trans to the CR ligand. The coordination of CO stabilizes the 16e$^-$ cation **9a**, and compound **10** can be obtained as analytically pure material.

In contrast to **2a,** the cation **9a** is fairly inert. Reactions with donor ligands like $NCCH_3$ or $P(OMe)_3$ are too slow to allow for an isolation of possible reaction products from by-products and intermediates. As we have seen in the case of the triflate ion, the free coordination site is effectively shielded by the sterically demanding dppep ligand, and only small ligands like CO or Cl^- are able to coordinate to the tungsten center in **9a**.

2.4. Bonding characteristics of $[W(CR)(CO)L(PR_3)_2]^+$ complexes

To gain a deeper understanding of the complex formation chemistry of cation **2a**, calculations were performed on model compounds derived from the transition metal fragment $W(CH)(CO)_2(PH_3)_2$, [W]. The computational work parallels the reactivity studies undertaken with the novel tungsten cation, and it is sought to identify characteristic bonding properties, which might enable one to adjust and tune the course of conceivable catalytic conversions. Besides the tungsten carbyne chloride [W]–Cl (**I**), the 16e$^-$ cation [W]$^+$ (**II**$^+$), and the phosphonic ester complex [W]–$OPH(OMe)_2$ (**III**$^+$), a variety of donor adducts {[W]–L}$^+$ have been analyzed (L = PH_3 (**IIa**$^+$); PMe_3 (**IIb**$^+$); $P(OH)_3$ (**IIc**$^+$); $P(OMe)_3$ (**IId**$^+$); CO (**IIe**$^+$); NCMe (**IIf**$^+$); THF (**IIg**$^+$); CH_2Cl_2 (**IIh**$^+$); $OPH(OH)_2$ (**IIi**$^+$)) (Scheme 5).

The computational study is further extended to include the bimetallic model compound {[W]–Cl–[W]}$^+$ (**IV**$^+$).

2.4.1. Structure of selected model complexes

Two tungsten carbyne chloride complexes containing the dppe ligand are described structurally in the literature, namely *trans*-W(C(CCHR))Cl(CO)$_2$(dppe) (R = ⬡) [7] and *trans*-W(C(*p*-$C_6H_4NH_2$))Cl(CO)$_2$(dppe) [19]. In Fig. 3, we compare the crystallographic data of these compounds with the optimized structure of **I**. The coordination geometry around the tungsten center is well reproduced in the simplified model system. The deviations between measured and calculated W–L bond lengths are around 2 pm.

The structure of the [W]$^+$ fragment **II**$^+$, a model for the cation **2a**, is of square pyramidal coordination

geometry; the most significant change in the structure, when comparing to **I**, is a shortening of the W≡CH bond by 5 pm. We note further a slight contraction of the calculated d(CO) bond length, which is consistent with the high-field shift of the $\tilde{\nu}$(CO) stretching frequencies observed for **2a**. Also shown in Fig. 3 is a comparison of the solid state structure of **6a** with the optimized geometry of **III**$^+$. The calculated values for d(W–CR), d(W–CO) and d(W–P) are in fair agreement with the experimental data, whereas the W–O distance in **III**$^+$ is significantly longer by 7 pm compared to the cation in **6a**. The P=O double bond of the phosphonate ester elongates under coordination to the metal fragment, the distance d(P–O) for optimized free ligand amounts to 150 pm. The experimentally determined value for d(P–O) is slightly larger than that of free phosphonates (d(P–O) = 146 [20] and 145 pm [21]).

Selected geometric parameters for various {[W]–L}$^+$ complexes are collected in Table 1.

Inspection of the data reveals the fact that the coordination geometry of the phosphorus and the carbonyl framework is essentially the same for all complexes investigated. The W–CH distances vary between 181 and 184 pm. Both strong σ donors as well as π acceptors *trans* to the carbyne unit cause an elongation of the W≡CH bond, since both electrostatic effects as well as π-backdonation determine the tungsten–carbon triple bond strength. The phosphorus systems **IIa**$^+$**–IId**$^+$ all show deviations from linearity in the angles ∠(C_{CH}–W–L) and ∠(H–C_{CH}–W), which is most prominent for the trialkyl phosphine. This effect can be rationalized on the basis of particular orbital interactions that take place in the bonding between a PR_3 donor with a $16e^-$–ML_5 transition metal fragment [22].

The coordination of the ligand L^t *trans* to the carbyne group is of special interest. All systems, in which L^t is a phosphorus donor, show a prolonged W–P distance, a manifestation of the strong *trans* influence of the carbyne unit [3]. In complex **IId**$^+$, the weak bond of the CO^t group is indicated by the long W–(CO) distance, and the value of d(C≡O), which is identical to that optimized for the free ligand, implies that π-backbonding is of only minor importance. In the next section, we investigate the trends in bonding, which are suggested by the optimized geometries, in more detail.

2.4.2. Bond analysis for selected model compounds

We analyze the energy changes associated with the bond forming reaction as shown in Scheme 3, in terms of steric contributions ΔE^0 and orbital interactions ΔE_{int} [22,23]. The latter describe σ-donation and π-backdonation, whereas the former contain terms due to Pauli repulsion, as well as an electrostatic component ΔE_{elstat}. The two terms can be combined to give the ligand association energy ΔE_{LA}, which is related to the bond snapping energy BE_{snap},: $\Delta E_{LA} = \Delta E^0 + \Delta E_{int} = -BE_{snap}$. This value does not directly correlate with the reaction enthalpy at 0 K, since — besides zero point energy corrections —, a preparation energy term has to be taken into account. It is however related to metal–ligand bond enthalpy terms, which provide a better description for bond strengths than bond dissociation enthalpies do [24]. The bond energy *BE* is ob-

Table 1
Selected optimized bond distances (pm) and bond angles (°) bond energy terms (kJ mol^{-1}) and Hirshfeld charges (a.u.) for {[W]–L}$^+$ systems ([W] = [W(CH)(CO)$_2$(PH$_3$)$_2$])

L	**IIa**$^+$ PH_3	**IIb**$^+$ Pme_3	**IIc**$^+$ $P(OH)_3$	**IId**$^+$ $P(OMe)_3$	**IIe**$^+$ [a] CO	**IIf**$^+$ NCMe	**IIg**$^+$ THF	**IIh**$^+$ CH_2Cl_2	**IIi**$^+$ $OPH(OH)_2$	**III**$^+$ $OPH(OMe)_2$
d(W–L)	274	266	266	267	228	227	236	276	234	[b]
d(W–C_{CH})	183	184	183	183	184	183	182	181	181	[b]
d(W–C_{CO})	205	203	205	204	205	205	205	205	205	[b]
d(W–P)	253	252	253	253	254	253	254	254	254	[b]
∠(C^t–W–L)	175	168	175	172	179	179	176	179	179	179
∠(H–C–W)	179	171	178	174	179	180	179	180	179	179
ΔE_{elstat}	−188	−341	−251	−283	−207	−245	−183	−94	−180	−202
ΔE^0	35	30	18	35	74	−1	−9	32	−25	−31
ΔE_{int}	−152	−241	−178	−207	−172	−151	−118	−101	−120	−134
BE_{snap}	117	211	160	172	98	152	127	69	145	165
BE	107	182	140	140	88	145	116	58	130	147
q_H([W])	0.87	0.77	0.89	0.83	1.01	0.90	0.86	0.88	0.87	0.85
q_H(L)	0.13	0.23	0.11	0.17	−0.01	0.10	0.14	0.12	0.13	0.15

[a] d(C–O)$_{CO}$ = 115 pm, d(C–O)$_L$ = 114 pm.
[b] See Fig. 3.

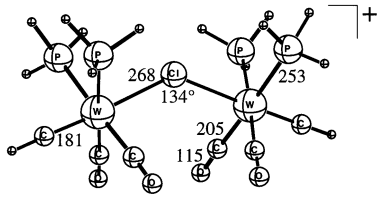

IV$^+$

Fig. 4. Calculated structure of the cation $[\{W(CH)(CO)_2(PH_3)_2\}_2(\mu\text{-}Cl)]^+$ (**IV**$^+$). Distances and angles are reported in pm and degrees, respectively.

tained when BE_{snap} is corrected by the preparation energy, $BE = BE_{snap} - \Delta E_{prep}$. It is further instructive to analyze the charge distribution on the interacting fragments. The Hirshfeld charges [25] q_H provide a measure for the charge flow as it occurs during bond formation.

The results of our analysis are collected in Table 1. Among the systems where L is a phosphorus donor, **IIa**$^+$–**IId**$^+$, the trialkyl substituted donor undergoes by far the strongest interaction with the metal center, both in terms of electrostatic as well as orbital interactions. This can also be seen in the charge distribution which show the largest amount of charge transfer for **IIb**$^+$. Of two phosphite ligands, the $P(OMe)_3$ molecule posses the higher W–L bond strength, mainly caused by an increase in the orbital interaction term. However, due to the difference in $-\Delta E_{prep}$, the bond energy terms BE are similar for both $P(OMe)_3$ and $P(OH)_3$.

When we compare the two system with L^t ligands able of π-backbonding, we find in the case of CO a weak W–L bond, although the orbital interaction term is fairly large, and comparable to that of some phosphorus donors. The large destabilizing ΔE^0 contribution substantially weakens the metal carbonyl bond. We further observe that no net charge low takes place in the formation of **IIe**$^+$. The situation is different for the acetonitrile ligand. The electrostatic contribution to the W–L bond removes the antibonding character from the steric term ΔE^0, and as a consequence leads to the formation of a stable W–(NCMe) bond. The π contributions for both ligands amount to about 35% of the term ΔE_{int}, and do not represent the dominant orbital interaction.

The weak W–(CO^t) bond provides a rationale for the fact that in **3** a phosphorus donor occupies the coordination site *trans* to the carbyne group. We have calculated that the isomerization *mer*-**IId**$^+ \rightarrow$ *fac*-**IId**$^+$ is energetically favorable by 34 kJ mol^{-1}. The d(CO) values in *fac*-**IId**$^+$ are 207 and 209 pm; about 2–4 pm longer than the average calculated d(CO) distance (compare the entries in Table 1). Both changes in ΔE_{int} and ΔE^0 contribute to the stabilization energy, the changes in the steric term being the more important ones.

Lastly, we analyze the complexes containing ligand capable of π-donation. For all complexes **IIg**$^+$–**IIi**$^+$ and **III**$^+$, the orbital interaction terms are comparable, and it is again the influence of the electrostatic interaction term that in most of the cases, except for **IIh**$^+$, causes a bonding ΔE^0 contribution, and a fairly stable metal to ligand bond. The weak W–L bond of the non-coordinating solvent ligand is caused not by a comparatively small orbital interaction term, but is due to the steric repulsion. In the $OPH(OR)_2$ systems, the substitution of hydrogen by methyl groups leads to increase in W–L bond strength of about 20 kJ mol^{-1}. The fact that, in terms of *BE*, the W–L linkage is somewhat stronger in **III**$^+$ than in **IId**$^+$, might contribute to the driving force for the Arbuzov dealkylation as observed in the experiment.

2.4.3. The {[W]–Cl–[W]}$^+$ cation

In Fig. 4, the optimized structure of the bimetallic cation **IV**$^+$ is displayed. The geometry of the two [W] fragments is similar to those found for the complexes described before. The molecule possesses C_{2v} symmetry; calculations in which this symmetry constrained is lifted did not result in structures with significantly varying W≡C or W–CO bond lengths, as observed in the crystal structure. The large differences in the distances W(1)–C(1) and W(1)–C(2) or W(1)–C(5) and W(2)–C(6) observed for **7** (compare Fig. 2), are probably due to the poor quality of the crystal used for the structure determination (see experimental section).

For the geometry around the bridging μ-Cl ligand, we find W–Cl distances of 268 pm, which is 6 pm longer than in the crystal structure, and an angle ∠(Cl–W–Cl) of 134°, which is opened up by 8° compared to **7**. We have found similar discrepancies between calculated and observed M–Cl distances in cationic {[Zr]–Cl–[Zr]}$^+$ systems [26]. A theoretical analysis revealed that the potential surface for internal coordinates involving the μ–Cl group is very shallow, and that external effects like the presence of counterions may have a profound influence on the bridging geometry.

For model compound **IV**$^+$, we also find very soft W–Cl stretching, and W–Cl–W bending modes. A geometric arrangement with differences in W–Cl bond lengths of 2 pm (d(W–Cl) = 267, 269 pm) is less than 1 kJ mol^{-1} higher in energy. The distortion of the optimized structure to adapt a μ-Cl geometry as found in the crystal requires only 6 kJ mol^{-1}. Introduction of a negative point charge q^-, being 700 pm away from one tungsten center, and located in the W–Cl–W mirror plane, the W–Cl and W-q^- vectors being perpendicular, reduces the symmetry of the molecular system to C_s, and causes an elongation of the adjacent W–Cl bond by 2 pm, but a contraction of the distant W–Cl bond by 6 pm. The asymmetric μ-Cl coordination of the cation **7**$^+$ as deduced from the NMR spectra might therefore be caused by the presence of outer ion pairs in solution.

The analysis for the bond forming reaction [W]–Cl + $[W]^+ \rightarrow \{[W]–Cl–[W]\}^+$ reveals a strong W–Cl bond with a value for BE_{snap} of 164 kJ mol^{-1}. The bond energy *BE* reduces to 147 kJ mol^{-1}, but is still comparable to that of systems with phosphorus donors. The Hirshfeld charges of $q_H([W]) = 0.81$ and $q_H(L) = 0.19$ a.u. indicate that charge delocalization is a stabilizing factor in bond formation. This fact is also reflected in the q_H values for the tungsten atoms in **I**, $\mathbf{II}^+$ and $\mathbf{IV}^+$, which amount to 0.10, 0.23, and 0.11 a.u., respectively.

3. Conclusion

In this work, we have described a synthetic route to the tungsten carbyne cations $[W(CMes)(CO)_2(dppe)]^+$ and $[W(CMes)(CO)(dppep)]^{+\cdot}$ Preliminary reactivity studies have been performed in reactions with donor ligands. A theoretical analysis rationalizes the trends observed in theses experiments, and reveals the importance of steric effects, especially of electrostatic nature, for the metal to ligand bonding interaction.

4. Experimental

4.1. Preparative procedures

All manipulations were performed under a nitrogen atmosphere using standard Schlenk techniques. Solvents were dried according to standard procedures, and distilled under N_2 prior to use. The complexes *trans*-$W(CMes)Cl(CO)_2(dppe)$ (**1**) and *trans*-$W(CMes)Cl(CO)(dppep)$ (**8**) were prepared as described elsewhere [3]. PMe_3 [27] and PEt_3 [28] were synthesized following slightly modified literature procedures [29], whereas all other reagents were purchased and used without further purification. The following instruments were used for spectroscopic and physical characterization: Varian Gemini 200 and Gemini 300 NMR spectrometers. ^1H and ^{13}C chemical shifts are referred to Me_4Si and referenced through the residual proton or ^{13}C resonances of the deuterated solvent. ^{31}P chemical shifts were externally referenced to 85% H_3PO_4. Bio-Rad FTS-45 IR spectrometer. Finnigan/MAT 8320 mass spectrometer. LECO CHNS-932 for elemental analyses.

4.1.1. $[W(CMes)(CO)_2(dppe)][SbF_6]$ (**2a**)

To a solution of **1** (1g, 1.24 mmol) in CH_2Cl_2 (30 ml), $AgSbF_6$ (0.64 g, 1.86 mmol), dissolved in CH_2Cl_2 (30 ml), was added at room temperature (r.t.). AgCl precipitated immediately. It was stirred for 10 min under the exclusion of light, and the solvent was removed in vacuo. The solid was suspended in benzene (60 ml), and the remanining silver salts were filtered off through Celite. The clear, yellowish–red solution was evaporated in vacuo, the yellow residue dissolved in CH_2Cl_2, and precipitated with hexane. After several precipitations, **2a** (1.13 g, 1.13 mmol, 91%) was obtained as yellow powder. IR (KBr, cm^{-1}): 2000 (s), 1931 (s). ^1H-NMR (300 MHz, CD_2Cl_2, ppm): 7.8–7.55 (m, 8H, Ph), 7.40–7.10 (m, 12H, Ph), 6.83 (s, 2H, Mes), 3.10–2.80 (m, 4H, PCH_2), 2.13 (s, 6H, CH_3-Mes), 2.11 (s, 3H, CH_3-Mes). $^{13}C\{^1H\}$-NMR (75.4 MHz, CD_2Cl_2, ppm): 217.5 (dd, $^2J_{CP} = 36.3 \times 5.0$ Hz, CO), 25.8–25.0 (m, CH_2–dppe), 21.7 (s, CH_3–Mes), 20.5 (s, $2CH_3$–Mes). Due to decompostion of **2a**, the remaining carbon atoms could not be assigned with certainty. $^{13}C\{^1H\}$-NMR (75.4 MHz, d_8-THF, ppm): 300 (m, *C*Mes), 219.3 (dd, $^2J_{CP} = 37.4 \times 7.9$ Hz, CO). $^{31}P\{^1H\}$-NMR (121.5 MHz, CD_2Cl_2, ppm): 50.7 (s, $^1J_{PW} = 237$ Hz). MS (FAB-Neg, LM = CH_2Cl_2, M = NBOH, *e*/*z*, %): 769 (M^+, 100), 741 ($M^+ - CO$, 20), 713 ($M^+ - 2$ CO, 18). Anal. for $C_{38}H_{35}F_6O_2P_2SbW$ (1005.23). Calc. C (45.40), H (3.51); Found: C (45.69), H (4.15)%.

4.1.2. $W(CMes)(CO)_2(dppe)(OTf)$ (**2b**)

A solution of **1** (1.12g, 1.39 mmol) in CH_2Cl_2 (60 ml), was treated with a solution AgOTf (0.54 g, 2.09 mmol) in CH_2Cl_2 (30 ml). Immediate precipitation of AgCl occured. After stirring for 3 h under the exclusion of light, the reaction mixture was evaporated in vacuo, and the resulting yellowish–brown solid was suspended in a small amount of benzene, followed by filtration through celite and removal of the solvent. Recrystallization from CH_2Cl_2/hexane afforded **2b** (1.14 g, 1.24 mmol) as yellow powder. IR (KBr, cm^{-1}): 1998 (s), 1932 (s). ^1H-NMR (300 MHz, CD_2Cl_2, ppm): 7.85–7.75 (m, 4H, Ph), 7.70–7.60 (m, 4H, Ph), 7.50–7.20 (m, 12H, Ph), 6.55 (s, 2H, Mes), 3.12–2.92 (m, 2H, PCH_2), 2.90–2.70 (m, 2H, PCH_2), 2.15 (s, 3H, CH_3–Mes), 1.82 (s, 6H, CH_3–Mes). $^{13}C\{^1H\}$-NMR (75.4 MHz, CD_2Cl_2, ppm): 289.6 (t, $^2J_{CP} = 7.9$ Hz, *C*Mes), 216.4 (dd, $^2J_{CP} = 40.4 \times 7.2$ Hz, CO), 143.6 (s, *ipso*-Mes), 139.4 (s, *o*-Mes), 134.3 (s, *p*-Mes), 128.3 (s, *m*-Mes), 133.4, 133.2, 132.2, 132.1, 131.7, 131.4, 130.7, 129.4, 129.3, 129.2 (C_6H_5), 118.7 (q, $^1J_{CF} = 319.5$ Hz, CF_3), 25.8 (dd, $^1J_{CP} = 27.4$ Hz, $^2J_{CP} = 11.7$ Hz, PCH_2), 21.5 (s, CH_3–Mes), 20.2 (s, $2CH_3$–Mes). ^{19}F-NMR (282.3 MHz, CD_2Cl_2, ppm): −78.0 (s). $^{31}P\{^1H\}$-NMR (121.5 MHz, CD_2Cl_2, ppm): 46.8 (s, $^1J_{PW} = 239$ Hz). MS (FAB-Neg, LM = CH_2Cl_2, M = NBOH, *e*/*z*, %): 920 (M^+, 1), 769 ($M^+ - SO_3CF_3$, 100), 741 ($M^+ - SO_3CF_3 - CO$, 30), 712 ($M^+ - SO_3CF_3 - 2$ CO, 10). Anal. for $C_{39}H_{35}F_3O_5P_2SW$ (918.11). Calc. C (50.97), H (3.84); Found: C (51.23), H (3.91)%.

4.1.3. $[W(CMes)(CO)_3(dppe)][SbF_6]$ (**3**)

To a solution of **1** (2.01g, 2.50 mmol) in CH_2Cl_2 (60 ml), $AgSbF_6$ (1.28 g, 3.75 mmol), dissolved CH_2Cl_2 (30

ml), was added at r.t. under an atmosphere of carbon monoxide. Stirring for 30 min under the exclusion of light was followed by evaporation of the solvent. The residue was suspended in benzene and filtered through Celite. The clear, yellow filtrate was evaporated in vacuo, and the solid washed with the hexane. Compound **3** (2.46 g, 2.38 mmol, 95%) was isolated as yellow powder. IR (KBr, cm^{-1}): 2074 (w), 1993 (s), 1922 (s). ^{1}H-NMR (300 MHz, CD_2Cl_2, ppm): 7.55–7.40 (m, 20H, Ph), 6.80 (s, 2H, Mes), 3.10–2.80 (m, 4H, PCH_2), 2.22 (s, 3H, C*H*$_3$–Mes), 2.20 (s, 6H, C*H*$_3$–Mes). ^{13}C{^{1}H}-NMR (75.4 MHz, CD_2Cl_2, ppm): 308.8 (dd, $^2J_{CP} = 20.1 \times 7.8$ Hz, *C*Mes), 205.0 (dd, $^2J_{CP} = 21.9 \times 8.3$ Hz, CO), 201.5 (t, $^2J_{CP} = 7.3$ Hz, 2CO), 145.1 (s, *ipso*-Mes), 144.1 (s, *o*-Mes), 133.7 (s, *p*-Mes), 129.6 (s, *m*-Mes), 132.3, 132.2, 132.1, 131.9, 130.6, 130.4, 130.1, 129.9 (C_6H_5), 29.7 (dd, $^1J_{CP} = 30.1$ Hz, $^2J_{CP} = 13.3$ Hz, PCH_2), 26.6 (dd, $^1J_{CP} = 26.1$ Hz, $^2J_{CP} = 9.8$ Hz, PCH_2), 22.2 (s, *C*H$_3$–Mes), 21.0 (s, 2*C*H$_3$–Mes). ^{31}P{^{1}H}-NMR (121.5 MHz, CD_2Cl_2, ppm): 37.9 (s, 1P, $^1J_{PW} = 237$ Hz), 23.9 (s, 1P, $^1J_{PW} = 91$ Hz). MS (FAB-Neg, LM = CH_2Cl_2, M = NBOH, *e*/*z*, %): 797 (M^+, 50), 769 ($M^+ - CO$, 60), 741 ($M^+ - 2CO$, 20), 713 ($M^+ - 3CO$, 13). Anal. for $C_{39}H_{35}F_6O_3P_2SbW \cdot 2C_6H_6$ (1033.25). Calc. C (51.50), H (3.98); Found: C (51.34), H (4.12)%.

4.1.4. [W(CMes)(OC$_4$D$_8$)(CO)$_2$(dppe)][SbF$_6$] (**4a**)

In an NMR tube, **2a** (82 mg, 81.8 mmol) was dissolved in d_8-THF (0.5 ml). After a few minutes at r.t., a stable distribution of compounds **2a**, **3** and **4a** was obtained. The ratio of these complexes as determined by ^{31}P{^{1}H}-NMR spectroscopy was 3:1:2. **4a** could not be isolated by precipitation, crystallization, or evaporation of the solvent, and was therefore characterized by NMR spectroscopy of the reaction mixture. ^{1}H-NMR (300 MHz, d_8-THF, ppm): 6.53 (s, 2H, Mes), 2.05 (s, 3H, C*H*$_3$-Mes), 1.77 (s, 6H, C*H*$_3$–Mes). ^{13}C{^{1}H}-NMR (75.4 MHz, d_8-THF, ppm): 218.5 (dd, $^2J_{CP} = 38.2 \times 7.2$ Hz, CO), 70.2 (quint, O*C*D$_2$CD$_2$), 26.4 (quint, OCD$_2$*C*D$_2$).^{31}P{^{1}H}-NMR (121.5 MHz, d_8-THF, ppm): 47.1 (s, $^1J_{PW} = 235$ Hz).

4.1.5. [W(CMes)(CH$_3$CN)(CO)$_2$(dppe)][SbF$_6$] (**4b**)

A solution of **2a** (0.5 g, 0.62 mmol) in CH_2Cl_2 (15 ml) and CH_3CN (5 ml) was treated with a solution of $AgSbF_6$ (0.28 g, 0.81 mmol) in CH_2Cl_2 (15 ml). After stirring for 2 h under exclusion of light, the resulting yellow suspension was evaporated in vacuo. The dark-yellow solid was suspended in benzene (35 ml) and filtered through Celite. The solvent was removed, and the raw product recrystallized from CH_2Cl_2/hexane. **4b** (0.61 g, 0.58 mmol, 94%) was obtained as yellow–orange powder. IR (KBr, cm^{-1}): 2005 (s), 1935 (s). ^{1}H-NMR (300 MHz, CD_2Cl_2, ppm): 7.90–7.20 (m, 20H, Ph), 6.63 (s, 2H, Mes), 3.30–2.80 (m, 4H, PCH_2), 2.19 (s, 3H, C*H*$_3$–Mes), 1.90 (s, 6H, C*H*$_3$–Mes), 1.45 (s, 3H, CH_3CN). ^{13}C{^{1}H}-NMR (75.4 MHz, CD_2Cl_2, ppm): 296.0 (t, $^2J_{CP} = 8.4$ Hz, *C*Mes), 214.9 (dd, $^2J_{CP} = 32.6 \times 7.4$ Hz, CO), 143.2 (s, *ipso*-Mes), 142.0 (s, *o*-Mes), 141.2 (s, *p*-Mes), 128.6 (s, *m*-Mes), 133.5, 133.2, 131.9, 131.6, 131.4, 131.2, 130.0, 129.8, 129.6, 129.4, (C_6H_5, CH_3CN), 26.1 (dd, $^1J_{CP} = 29.4$ Hz, $^2J_{CP} = 10.9$ Hz, PCH_2), 21.7 (s, *C*H$_3$-Mes), 20.5 (s, 2*C*H$_3$-Mes), 2.1 (s, *C*H$_3$CN). ^{31}P{^{1}H}-NMR (121.5 MHz, C_6D_6, ppm): 46.3 (s, $^1J_{PW} = 232$ Hz). MS (FAB-Neg, LM = CH_2Cl_2, M = NBOH, *e*/*z*, %): 810 (M^+, 1), 770 ($M^+ - CH_3CN$, 100), 741 ($M^+ - CH_3CN - CO$, 15), 713 ($M^+ - CH_3CN - 2CO$, 8). Anal. for $C_{40}H_{38}NF_6O_2P_2SbW \cdot CH_2Cl_2$ (1046.28): Calc. C (43.53), H (3.56), N (1.24); Found: C (43.63), H (4.17), N (0.87)%.

4.1.6. [W(CMes)(CO)$_2$(PMe$_3$)(dppe)][SbF$_6$] (**5a**)

At −20°C, PMe_3 (83 μl, 0.76 mmol) was added to a solution of **2a** (0.63 g, 0.63 mmol) in toluene (40 ml). The reaction mixture was allowed to warmed up to r.t. for 1 h. After stirring for 30 min, the solvent was removed in vacuo, and the resulting solid washed with hexane (5 ml). **5a** (0.51 g, 0.47 mmol, 75%) is isolated as dark-yellow powder by precipitation with hexane from a solution of the raw product in CH_2Cl_2. Repeated precipitation yielded analytically pure material. IR (KBr, cm^{-1}): 1992 (s), 1921 (s). ^{1}H-NMR (300 MHz, C_6D_6, ppm): 7.90–7.80 (m, 4H, Ph), 7.75–7.65 (m, 4H, Ph), 7.30–7.20 (m, 4H, Ph), 7.15–6.90 (m, 4H, Ph), 6.85–6.75 (m, 4H, Ph), 6.36 (m, 2H, Mes), 3.5–3.25 (m, 2H, PCH_2), 3.05–2.80 (m, 2H, PCH_2), 1.98 (s, 3H, C*H*$_3$–Mes), 1.82 (s, 6H, C*H*$_3$–Mes), 0.29 (d, 9H, PMe_3). ^{13}C{^{1}H}-NMR (50.3 MHz, CD_2Cl_2, ppm): 300.8 (m, *C*Mes), 214.6 (dt, $^2J_{CP} = 26.1 \times 7.3$ Hz, CO), 143.9 (s br, *ipso*-Mes), 142.6 (s, *o*-Mes), 135.1 (s br, *p*-Mes), 129.1 (s, *m*-Mes), 133.7, 133.2, 132.3, 132.0, 131.8, 131.4, 130.6, 130.0, 129.5, 129.2 (C_6H_5), 25.4 (dd, $^1J_{CP} = 30.0$ Hz, $^2J_{CP} = 11.9$ Hz, PCH_2), 21.9 (s, *C*H$_3$–Mes), 20.4 (s, 2*C*H$_3$–Mes), 17.1 (m br, PMe_3). ^{31}P{^{1}H}-NMR (121.5 MHz, C_6D_6, ppm): 38.6 (d, 2P, $^2J_{PP} = 22.3$ Hz, $^1J_{PW} = 227$ Hz), −58.9 (t, 1P, $^2J_{PP} = 22.3$ Hz, $^1J_{PW} = 83$ Hz). MS (FAB-Neg, LM = CH_2Cl_2, M = NBOH, *e*/*z*, %): 845 (M^+, 20), 818 ($M^+ - CO$, 10), 795 ($M^+ - 2CO$, 60), 769 ($M^+ - PMe_3$, 80), 742 ($M^+ - PMe_3 - CO$), 30), 714 ($M^+ - PMe_3 - 2CO$, 20). $C_{41}H_{44}F_6O_2P_3SbW$ (1081.32): Ber. C (45.54), H (4.10); Gef. C (45.56), H (4.12)%.

4.1.7. [W(CMes)(CO)$_2$(PEt$_3$)(dppe)][SbF$_6$] (**5b**)

As described for **5a**, **2a** (0.82 mg, 0.82 mmol) was reacted with PEt_3 (181 μl, 1.23 mmol) in toluene (60 ml) at −20°C. **5b** was obtained in 68% yield as dark-yellow powder. IR (KBr, cm^{-1}): 1990 (s), 1920 (s). ^{1}H-NMR (300 MHz, C_6D_6, ppm): 7.92–7.62 (m, 8H, Ph), 7.32–7.22 (m, 4H, Ph), 7.15–6.95 (m, 4H, Ph), 6.85–6.73 (m,

4H, Ph), 6.30 (m, 2H, Mes), 1.97 (s, 3H, CH_3–Mes), 1.89 (m, 12H, PCH_2CH_3), 1.86 (s, 6H, CH_3–Mes), 0.73 (m, 18H, PCH_2CH_3). $^{13}C\{^1H\}$-NMR (75.4 MHz, CD_2Cl_2, ppm): 301.6 (dt, $^2J_{CP} = 21.3 \times 8.8$ Hz, *C*Mes), 215.0 (dt, $^2J_{CP} = 26.8 \times 7.9$ Hz, CO), 143.0 (s, *ipso*-Mes), 138.2 (s, *o*-Mes), 135.0 (s, *p*-Mes), 128.5 (s, *m*-Mes), 133.7, 133.2, 132.3, 132.0, 131.8, 131.4, 130.6, 130.0, 129.5, 129.2 (C_6H_5), 25.9 (dd, $^1J_{CP} = 28.3$ Hz, $^2J_{CP} = 11.9$ Hz, PCH_2), 21.8 (s, *C*H_3–Mes), 20.9 (s, 2*C*H_3–Mes), 21.0 (m, P*C*H_2CH_3), 8.0 (s br, PCH_2CH_3). $^{31}P\{^1H\}$-NMR (121.5 MHz, C_6D_6, ppm): 38.1 (d, 2P, $^2J_{PP} = 21.5$ Hz, $^1J_{PW} = 226$ Hz), −26.2 (t, 1P, $^2J_{PP} = 21.5$ Hz, $^1J_{PW} = 84$ Hz).

4.1.8. [W(CMes)(CO)$_2$(OPH(OMe)$_2$)(dppe)][SbF$_6$] (6a)

Following the procedure for **5a**, **2a** (0.56 g, 0.56 mmol) was reacted with $P(OMe)_3$ (79 μl, 0.67 mmol) in toluene (20 ml). Recrystallization from CH_2Cl_2/hexane afforded **6a** (0.57 g, 0.48 mmol, 86%) as yellow, crystalline product. IR (KBr, cm^{-1}): 2000 (s), 1929 (s), 1050 (m, PO). ^{1}H-NMR (300 MHz, d_8-THF, ppm): 7.90–7.80 (m, 4H, Ph), 7.82–7.73 (m, 4H, Ph), 7.51–7.20 (m, 12H, Ph), 6.65 (s, 0.5H, OP*H*$(OMe)_2$, $^1J_{HP} = 752$ Hz), 6.60 (s, 2H, Mes), 4.13 (s, 0.5H, OP*H*$(OCH_3)_2$, $^1J_{HP} = 752$ Hz), 3.18 (d, $^2J_{HP} = 12.6$ Hz, 6H, OPH(O*Me*)$_2$), 3.10–2.90 (m br, 2H, PCH_2), 2.38–2.20 (m br, 2H, PCH_2), 2.14 (s, 3H, C*H*$_3$–Mes), 1.86 (s, 6H, C*H*$_3$–Mes). $^{13}C\{^1H\}$-NMR (75.4 MHz, CD_2Cl_2, ppm): 272.1 (t, $^2J_{CP} = 9.2$ Hz, *C*Mes), 216.1 (dd, $^2J_{CP} = 43.2 \times 6.6$ Hz, CO), 144.1 (s, *ipso*-Mes), 138.2 (s, *o*-Mes), 134.7 (s, *p*-Mes), 133.6, 133.4, 132.6, 132.4, 130.8, 130.1, 129.3, 129.0, 128.9, 128.7, 128,5 (C_6H_5), 128.2 (s, *m*-Mes), 54.3, 53.8, 53.3 (s, OPH$(OMe)_2$), 25.9 (dd, $^1J_{CP} = 27.1$ Hz, $^2J_{CP} = 12.4$ Hz, PCH_2), 21.5 (s, 1*C*H_3-Mes), 20.3 (s, 2*C*H_3–Mes). $^{31}P\{^1H\}$-NMR (121.5 MHz, C_6D_6, ppm): 49.0 (d, 2P, $^2J_{PP} = 5.6$ Hz, $^1J_{PW} = 236$ Hz, dppe), 19.1 (t, 1P, $^2J_{PP} = 5.6$ Hz, OPH$(OMe)_2$). ^{31}P-NMR (121.5 MHz, CD_2Cl_2, ppm): 49.2 (m br, 2P, dppe), 17.6 (dm, $^1J_{PH} = 752$ Hz, 1P, OPH$(OMe)_2$). MS (FAB-Neg, LM = CH_2Cl_2, M = NBOH, *e*/*z*, %): 879 (M^+, 37), 769 ($M^+ -$ OPH$(OMe)_2$, 100), 741 ($M^+ -$ OPH$(OMe)_2 -$ CO, 80), 712 ($M^+ -$ OPH$(OMe)_2 -$ 2CO, 25). Due to varying amounts of CH_2Cl_2 inclusions, it was not possible to obtain a reproducible elemental analysis.

4.1.9. W(CMes)(CO)$_2$(OPH(OEt)$_2$)(dppe)][SbF$_6$] (6b)

At −40°C, $P(OEt)_3$ (125 μl, 0.72 mmol) was added to a solution of **3** (0.62 g, 0.60 mmol) in CH_2Cl_2 (30 ml). The reaction mixture was allowed to warmed up to r.t. for 1 h, and was stirred over night. Evaporation in vacuo afforded a yellow oil, which was extracted with ether. **6b** (0.58 g (0.47 mmol, 78%) was isolated as yellow oil. IR (KBr, cm^{-1}): 2001 (s), 1933 (s), 1023 (s, PO).^{1}H-NMR (300 MHz, C_6D_6, ppm): 7.90–7.80 (m, 4H, Ph), 7.75–7.68 (m, 4H, Ph), 7.40–6.80 (m, 12H, Ph), 6.65 (s, 0.5H, OP*H*$(OEt)_2$, $^1J_{HP} = 748$ Hz), 6.38 (s, 2H, Mes), 4.16 (s, 0.5H, OP*H*$(OEt)_2$, $^1J_{HP} = 748$ Hz), 3.25–3.13 (m, 4H, OPH$(OCH_2CH_3)_2$), 2.75–2.50 (m br, 2H, PCH_2), 2.38–2.20 (m br, 2H, PCH_2), 2.10 (s, 3H, C*H*$_3$–Mes), 1.93 (s, 6H, C*H*$_3$–Mes), 0.79 (t, 6H, OPH$(OCH_2CH_3)_2$). $^{13}C\{^1H\}$-NMR (75.4 MHz, d_8-Toluol, ppm): 289.2 (m, *C*Mes), 218.1 (dd, $^2J_{CP} = 40.3 \times 7.2$ Hz, CO), 143.9 (s, *ipso*-Mes), 141.6 (s, *o*-Mes), 139.3 (s, *p*-Mes), 133.6, 133.4, 132.6, 132.4, 130.8, 130.1, 129.3, 129.0, 128.9, 128.7, 128.5 (C_6H_5), 128.7 (s, *m*-Mes), 64.5 (d, $^2J_{CP} = 5.8$ Hz, OPH$(OCH_2CH_3)_2$), 24.9 (dd, $^1J_{CP} = 28.6$ Hz, $^2J_{CP} = 11.4$ Hz, PCH_2), 21.8 (s, 1*C*H_3–Mes), 20.7 (s, 2*C*H_3–Mes) 15.6 (d, $^3J_{CP} = 7.3$ Hz, OPH$(OCH_2CH_3)_2$). $^{31}P\{^1H\}$-NMR (121.5 MHz, C_6D_6, ppm): 48.7 (d, 2P, $^2J_{PP} = 6.3$ Hz, $^1J_{PW} = 236$ Hz, dppe), 15.4 (t, 1P, $^2J_{PP} = 6.3$ Hz, OPH$(OEt)_2$).

4.1.10. [{W(CMes)(CO)$_2$(dppe)}$_2$Cl][SbF$_6$] (7)

$AgSbF_6$ (0.26 g, 0.75 mmol) was added to a solution of **2a** (1.2 g, 1.49 mmol) in CH_2Cl_2. AgCl started to precipitate, and after 5min, the solvent was removed in vacuo. The resulting yellowish–grey solid was suspendend in benzene (20 ml), and filtered through Celite. Precipitation with hexane afforded a yellow solid; a mixture of the compounds **1**, **2a**, **3** and **7**. Compound **7** crystallizes in large, colorless crystals from a benzene solution of the product mixture. It was not possible to obtain a pure solution of **5**. The crystals are extremely air sensitive, and decompose even under N_2 in the absence of benzene. IR (C_6H_6, cm^{-1}): 2007 (s), 1940 (s). ^{1}H-NMR (300 MHz, CD_2Cl_2, ppm): 6.47 (s, 2H, Mes), 2.11 (s, 6H, C*H*$_3$–Mes), 1.79 (s, 3H, C*H*$_3$–Mes). $^{13}C\{^1H\}$-NMR (75 MHz, CD_2Cl_2, ppm): 216.7 (dd, $^2J_{CP} = 38.9 \times 6.9$ Hz, CO) The resonances of the remaining carbon atoms could not be assigned with certainty. $^{31}P\{^1H\}$-NMR (121.5 MHz, d_8-Toluol, 45°C, ppm): 42.5 (s br, $^1J_{PW} = 230$ Hz). $^{31}P\{^1H\}$-NMR (121.5 MHz, d_8-Toluol, −75°C, ppm): 45.3 (s br, 2P, $^1J_{PW} = 232$ Hz), 40.8 (s br, 2P, $^1J_{PW} = 228$ Hz). $^{31}P\{^1H\}$-NMR (121.5 MHz, CD_2Cl_2, 25°C, ppm): 42.1 (s, $^1J_{PW} = 231$ Hz).

4.1.11. [W(CMes)(CO)({Ph$_2$PCH$_2$CH$_2$}$_2$PPh)][SbF$_6$] (9a)

$AgSbF_6$ (0.22 g, 0.63 mmol) was added to a solution of **8** (0.48 g, 0.53 mmol) in CH_2Cl_2 (60 ml). Immediately, AgCl started to precipitate. After 10 min, the reaction mixture was filtered through Celite. Addition of hexane to the clear filtrate yielded **9a** (0.48 g, 0.43 mmol, 82%) as yellow powder. IR (CH_2Cl_2, cm^{-1}): 1992 (s). ^{1}H-NMR (300 MHz, C_6D_6, ppm): 7.85–6.65 (m, 25H, Ph), 6.35 (s, 2H, Mes), 3.60–3.40 (m, 4H, PCH_2), 2.60–2.35 (m, 4H, PCH_2), 2.20 (s, 3H, C*H*$_3$–Mes), 1.81 (s, 6H, C*H*$_3$–Mes). $^{13}C\{^1H\}$-NMR (75.4 MHz, CD_2Cl_2, ppm): 316 (m, CMes), 218.8 (td, $^2J_{CP} =$

4.8 × 31.8 Hz, CO). $^{31}P\{^1H\}$-NMR (121.5 MHz, C_6D_6, ppm): 75.3 (t, 1P, $^2J_{PP} = 13.9$ Hz, $^1J_{PW} = 195$ Hz), 38.1 (d, 2P, $^2J_{PP} = 13.9$ Hz, $^1J_{PW} = 260$ Hz).

4.1.12. [W(CMes)(CO)({$Ph_2PCH_2CH_2$}$_2$PPh)][OTf] (9b)

Following the procedure for **9a**, the reaction of **8** (0.32 g, 0.35 mmol) with AgOTf (0.11 g, 0.42 mmol) afforded **9b** (0.33 g, 0.32 mmol, 91%) as yellow powder. IR (CH_2Cl_2, cm^{-1}): 1993 (s). ^1H-NMR (300 MHz, C_6D_6, ppm): 7.85–6.65 (m, 25H, Ph), 6.33 (s, 2H, Mes), 3.60–3.40 (m, 4H, PCH_2), 2.60–2.35 (m, 4H, PCH_2), 2.22 (s, 3H, CH_3–Mes), 1.81 (s, 6H, CH_3–Mes). $^{13}C\{^1H\}$-NMR (75.4 MHz, CD_2Cl_2, ppm): 316 (m, CMes), 218.8 (td, $^2J_{CP} = 4.8 \times 31.8$ Hz, CO). ^{19}F-NMR (282.3 MHz, CD_2Cl_2, ppm): −78.7 (s). $^{31}P\{^1H\}$-NMR (121.5 MHz, C_6D_6, ppm): 76.0 (t, 1P, $^2J_{PP} = 14.0$ Hz, $^1J_{PW} = 195$ Hz), 37.8 (d, 2P, $^2J_{PP} = 14.0$ Hz, $^1J_{PW} = 260$ Hz). MS (FAB-Neg, LM = THF, M = NBOH, e/z, %): 878 (M^+, 18), 850 ($M^+ - CO$, 40).

4.1.13. [W(CMes)(CO)$_2$({$Ph_2PCH_2CH_2$}$_2$PPh)][SbF_6] (10)

8 was reacted with 1.2 equivalents of $AgSbF_6$ in CH_2Cl_2 under 1 atm. of CO, yielding compound **10**. Analytically pure material was obtained by repeated precipitation with hexane from a CH_2Cl_2 solution. IR (KBr, cm^{-1}): 1994 (s), 1928 (s). ^1H-NMR (300 MHz, CD_2Cl_2, ppm): 7.95–6.90 (m, 25H, Ph), 6.61 (s, 2H, Mes), 3.40–2.10 (m, 8H, PCH_2), 2.19 (s, 3H, CH_3–Mes), 1.90 (s, 6H, CH_3–Mes). $^{13}C\{^1H\}$-NMR (75.4 MHz, CD_2Cl_2, ppm): 304.7 (m, CMes), 219.8 (td, $^2J_{CP} = 8.3 \times 15.4$ Hz, CO), 209.8 (td, $^2J_{CP} = 7.3 \times 25.7$ Hz). $^{31}P\{^1H\}$-NMR (121.5 MHz, C_6D_6, ppm): 68.7 (dd, 1P, $^2J_{PP} = 4.5 \times 1.6$ Hz, $^1J_{PW} = 226$ Hz), 41.0 (dd, 1P, $^2J_{PP} = 17.4 \times 4.5$ Hz, $^1J_{PW} = 223$ Hz), 21.0 (dd, 1P, $^2J_{PP} = 17.4 \times 1.6$ Hz, $^1J_{PW} = 75$ Hz). Anal. for $C_{46}H_{44}F_6O_2P_3SbW$ (1141.37): Calc. C (48.41), H (3.89); Found: C (48.30), H (3.85)%.

4.2. Crystal structure determination

Measurements were performed with a Siemens (Nicolet) R3m/V2000 diffractometer, using Mo–K_α radiation ($\lambda = 0.71073$ Å). For cell refinement and data reduction the program package SHELXTL-PC [30] was used, structure solution and structure refinement were accomplished using SHELXS [31] and SHELXL [32] software, respectively. Molecualr graphics have been prepared with PLATON [33].

4.2.1. Complex 5a

A yellow plate (0.20 × 0.20 × 0.08) was selected for the structure determination. Due to the relatively small size, and due to impurities in the crystalline material, the R-values are higher than expected. **5a** crystallizes from dichloromethane with one solvent molecule per asymmetric unit. The CH_2Cl_2 molecule and one methoxy oxygen atom appear to be disordered, and the respective Cl and O atoms were refined with the PART instructions in SHELXL-97. Positions of H atoms were calculated after each cycle of refinement (riding model) except for the hydrogen at P3, which has been located by difference electron density calculations. The positional parameters of this atom could not be refined and hence were fixed during the refinement. Crystal data: $C_{41}H_{44}Cl_2F_6NO_5P_3SbW$; $M = 1200.17$; triclinic, $a = 8.728(2)$, $b = 13.658(3)$, $c = 20.176(3)$ Å, $\alpha = 72.6(5)°$, $\beta = 79.2(5)°$, $\gamma = 84.41(2)°$; $V = 2253.2(8)$ Å^3; $T = 173(1)$ K, space group $P\bar{1}$, $Z = 2$, $\mu = 3.442$ mm^{-1}, 10476 reflections measured, 9817 unique ($R_{int} = 0.0488$), semi-emperical absorption correction; completeness to $\theta = 27°$: 99.8%; refined against F^2, final R indices ($I > 2\sigma(I)$): $R_1 = 0.0671$, $wR_2 = 0.1500$; final R indices (all data): $R_1 = 0.1086$, $wR_2 = 0.1744$.

4.2.2. Complex 7

The only suitable crystal for the X-ray experiment was of low quality with inclusion material. Therefore, the R-values are relatively high. However, the conformation of the tungsten moieties, which are bridged by a Cl atom, is well established. The counterion SbF_6^- appears to be disordered. Furthermore, five and a half benzene molecules per dimeric unit were found in difference Fourier maps. For some atoms, non-positive-definite anisotropic displacement parameters resulted in the refinement; which were then treated isotropically. For two benzene ring systems, distance restraints had to be applied. All positions of the H atoms were calculated after each cycle of refinement (riding model). Crystal data: $C_{109}H_{103}ClF_6O_4P_4SbW_2$; $M = 2239.69$; monoclinic, $a = 25.072(9)$, $b = 16.749(7)$, $c = 24.482(6)$ Å, $\beta = 105.680(10)°$; $V = 9898(6)$ Å^3; $T = 293(2)$ K, space group $P2_1/c$, $Z = 4$, $\mu = 2.744$ mm^{-1}, 12115 reflections measured, 11708 unique ($R_{int} = 0.1101$), numerical absorption correction; completeness to $\theta = 24°$: 72.5%; refined against F^2, final R indices ($I > 2\sigma(I)$): $R_1 = 0.0987$, $wR_2 = 0.2510$; final R indices (all data): $R_1 = 0.1857$, $wR_2 = 0.3076$.

4.3. Computational details

The ADF program package [34], release 1999.02, was used throughout this work, except for point-charge calculations, which were done as described elsewhere [26]. Self consistent GGA calculations have been performed, based on the LDA description by Vosko et al. [35] with gradient corrections due to Becke [36] and Perdew [37] (BP86). Use was made of the frozen core approximation. All elements except hydrogen have been described by a triple ζ-STO basis augmented by one d polarization function for the main group elements, or

by one $(n+1)$p function for the transition metal (ADF database IV). H-atoms were treated with a double ζ plus p basis set (ADF database III). Relativistic effects were included using a quasi-relativistic approach [38]. This is scheme has been applied successfully before to complexes of tungsten [39]. C_s or C_{2v} symmetry has been employed, except for model complexes **IIg**$^+$, **IIi**$^+$ and **III**$^+$ (no symmetry constraints).

5. Supplementary material

Crystallographic data for the structure analysis have been deposited with the Cambridge Crystallographic Data Centre, CCDC no. 143797 and CCDC no. 143798. Copies of this information may be obtained free of charge from The Director, CCDC, 12 Union Road, Cambridge CB2 1EZ UK (Fax: +44-1223-336033; e-mail: deposit@ccdc.cam.ac.uk or www: http://www.ccdc.cam.ac.uk).

Acknowledgements

Financial support from the Swiss National Science Foundation (SNSF) is gratefully acknowledged.

References

[1] (a) H. Fischer, P. Hofmann, F.R. Kreissl, R.R. Schrock, U. Schubert, K. Weiss, Carbyne Complexes, VCH, Weinheim, 1988. (b) A. Mayr, H. Hoffmeister, Adv. Organomet. Chem. 32 (1991) 227.
[2] F.W. Lee, M.C.W. Chan, K.K. Cheung, C.M. Che, J. Organomet. Chem. 552 (1998) 255.
[3] E. Bannwart, H. Jacobsen, F. Furno, H. Berke, Organometallics 19 (2000) 3605.
[4] (a) F. Furno, E. Bannwart, H. Berke, Chimia 53 (1999) 350. (b) F. Furno, T. Fox, H.W. Schmalle, H. Berke, Organometallics 19 (2000) 3620.
[5] (a) W. Koch, M.C. Holthausen, A Chemist's Guide to Density Functional Theory, Wiley–VCH, Weinheim, 2000. (b) J.F. Dobson, G. Vignale, M.P. Das (Eds.), Electronic Density Functional Theory: Recent Progress and New Directions, Plenum Press, New York, 1998. (c) H. Eschrig, The Fundamentals of Density Functional Theory, Teubner, Stuttgart, 1996. (d) J.M. Seminario (Ed.), Recent Developments and Applications of Modern Density Functional Theory, Elsevier, Amsterdam, 1996. (e) B.B. Laird, R.B. Ross, T. Ziegler (Eds.), Chemical Applications of Density Functional Theory, ACS Symposium Series 629, Washington, DC, 1996. (f) E.K.U. Gross, R.M. Dreizler (Eds.), Density Functional Theory, Plenum, New York, 1995. (g) N.H. March, Electron Density Theory of Atoms and Molecules, Academic Press, New York, 1992. (h) J. Labanowski, J. Andzelm (Eds.), Density Functional Methods in Chemistry, Springer, Heidelberg, 1991. (i) R.G. Parr, W. Yang, Density Functional Theory of Atoms and Molecules, Oxford University Press, Oxford, 1989.
[6] (a) K.R. Birdwhistell, S.J.N. Burgmayer, J.L. Templeton, J. Am. Chem. Soc. 105 (1983) 7789. (b) K.R. Birdwhistell, T.L. Tonker, J.L. Templeton, J. Am. Chem. Soc. 107 (1985) 4474.
[7] L. Zhang, M.P. Gamasa, J. Gimeno, R.J. Carbajo, F. Lopez-Ortiz, M. Lanfranchi, A. Tiripiccho, Organometallics 15 (1996) 4274.
[8] A.S. Goldman, K. Krogh-Jespersen, J. Am. Chem. Soc. 118 (1996) 12159.
[9] H. Jacobsen, H. Berke, T. Brackemeyer, T. Eisenblätter, G. Erker, R. Fröhlich, O. Meyer, K. Bergander, Helv. Chim. Acta 81 (1998) 1692.
[10] G.L. Hillhouse, B.L. Haymore, Inorg. Chem. 26 (1987) 1876.
[11] J.G. Verkade, L.D. Quin, Phosphorous-31 NMR Spectroscopy in Stereochemical Analysis, vol. 8, VCH, Weinheim, 1987.
[12] (a) R.V. Honeychuck, W.H. Hersh, Inorg. Chem. 28 (1989) 2869. (b) W.H. Hersh, J. Am. Chem. Soc. 107 (1985) 4599.
[13] K. Sünkel, U. Nagel, W. Beck, J. Organomet. Chem. 251 (1983) 227.
[14] D.H. Johnston, D.F. Shriver, Inorg. Chem. 32 (1993) 1045.
[15] A.G. Orpen, L. Brammer, F.H. Allen, O. Kennard, D.G. Watson, R. Taylor, J. Chem. Soc. Dalton Trans. (1989) S1.
[16] M.M. Crutchfield, C.H. Dungan, J.H. Letcher, V. Mark, J.R.V. Wazer, P31 Nuclear Magnetic Resonance, vol. 5, Interscience, New York, 1967.
[17] B.A. Arbuzov, Pure Appl. Chem. 9 (1964) 307.
[18] (a) D. Veghini, H. Berke, Inorg. Chem. 35 (1996) 4770. (b) G. Weiler, G. Huttner, L. Zsolnai, H.Z. Berke, Naturforsch. Teil B 42 (1987) 203.
[19] M.P.Y. Yu, A. Mayr, K.-K. Cheung, J. Chem. Soc. Dalton Trans. (1998) 475.
[20] W. Saenger, M. Mikolajczyk, Chem. Ber. 106 (1973) 3519.
[21] E. Müller, H.-B. Bürgi, Helv. Chim. Acta 70 (1987) 1063.
[22] (a) H.-B. Kraatz, H. Jacobsen, T. Ziegler, P.M. Boorman, Organometallics 12 (1993) 76. (b) H. Jacobsen, T. Ziegler, Comments Inorg. Chem. 17 (1995) 301.
[23] F.M. Bickelhaupt, E.J. Baerends, Rev. Comp. Ch. 15 (2000) 1.
[24] J.A.M. Martinho Simões, J.L. Beauchamp, Chem. Rev. 90 (1990) 629.
[25] F.L. Hirshfeld, Theor. Chim. Acta 44 (1977) 129.
[26] H. Jacobsen, T. Brackemeyer, H. Berke, G. Erker, R. Fröhlich, Eur. J. Inorg. Chem. (2000) 1423.
[27] W. Wolfsberger, H. Schmidbaur, Syn. React. Inorg. Met.-Org. Chem. 4 (1974) 149.
[28] M.L. Luetkens, A.P. Sattelberger, H.H. Murray, J.D. Basil, J.P. Fackler, Inorg. Synth. 29 (1990) 7.
[29] E. Bannwart, PhD Thesis, Universität Zürich, 1998.
[30] SHELXTL-PC, Siemens Analytical X-ray Instruments, Inc., 1990.
[31] G.M. Sheldrick, Acta Crystallogr. A46 (1990) 467.
[32] G.M. Sheldrick, SHELXL-97, Universität Göttingen, Germany, 1997.
[33] A.L. Spek, Acta Crystallogr. A46 (1990) C34.
[34] (a) E.J. Baerends, A. Bérces, C. Bo, P.M. Boerrigter, L. Cavallo, L. Deng, R.M. Dickson, D.E. Ellis, L. Fan, T.H. Fischer, C. Fonseca Guerra, S.J.A. van Gisbergen, J.A. Groeneveld, O.V. Gritsenko, F.E. Harris, P. van den Hoek, H. Jacobsen, G. van Kessel, F. Kootstra, E. van Lenthe, V.P. Osinga, P.H.T. Philipsen, D. Post, C.C. Pye, W. Ravenek, P. Ros, P.R.T. Schipper, G. Schreckenbach, J.G. Snijders, M. Sola, D. Swerhone, G. teVelde, P. Vernooijs, L. Versluis, O. Visser, E. van Wezenbeek, G. Wiesenekker, S.K. Wolff, T.K. Woo, T. Ziegler, ADF Release 1999.01/02, SCM, Amsterdam, 1999. (b) C.F. Guerra, J.G. Snijders, G. teVelde, E.J. Baerends, Theor. Chem. Acc. 99 (1998) 391.

[35] S.H. Vosko, L. Wilk, M. Nussair, Can. J. Phys. 58 (1980) 1200.
[36] A.D. Becke, Phys. Rev. A 38 (1988) 3098.
[37] J.P. Perdew, Phys. Rev. B 33 (1986) 8822.
[38] T. Ziegler, V. Tschinke, E.J. Baerends, J.G. Snijders, W. Ravenek, J. Phys. Chem. 93 (1989) 3050.
[39] (a) J. Li, G. Schreckenbach, T. Ziegler, J. Phys. Chem. 98 (1994) 4838. (b) H. Jacobsen, G. Schreckenbach, T. Ziegler, J. Phys. Chem. 98 (1994) 11406.